Hindawi Publishing Corporation
Journal of Nanomaterials
Volume 2014, Article ID 840102, 11 pages
http://dx.doi.org/10.1155/2014/840102

Research Article

Synthesis and Mechanism of Tetracalcium Phosphate from Nanocrystalline Precursor

Jianguo Liao,[1] Xingze Duan,[1] Yanqun Li,[1] Caifeng Zheng,[2] Zhengpeng Yang,[1] Aiguo Zhou,[1] and Dinghua Zou[1]

[1] *School of Materials Science and Engineering, Cultivating Base for Key Laboratory of Environment-Friendly Inorganic Materials in University of Henan Province, Henan Polytechnic University, Jiaozuo 454000, China*
[2] *Carbon/Carbon Composites Technology Research Center, Northwestern Polytechnical University, Xi'an 710072, China*

Correspondence should be addressed to Jianguo Liao; liaojianguo10@hpu.edu.cn

Received 23 July 2014; Revised 17 October 2014; Accepted 17 October 2014; Published 11 November 2014

Academic Editor: Christian Brosseau

Tetracalcium phosphate (TTCP, $Ca_4(PO_4)_2O$) was prepared by the calcination of coprecipitated mixture of nanoscale hydroxyapatite (HA, $Ca_{10}(PO_4)_6(OH)_2$) and calcium carbonate crystal ($CaCO_3$), followed by cooling in the air or furnace. The effect of calcination temperature on crystal structure and phase composition of the coprecipitation mixture was characterized by transmission electron microscope (TEM), thermal analysis-thermogravimetry (DTA-TG), X-ray diffraction (XRD), Fourier transform-infrared spectroscopy (FT-IR), and Raman spectroscopy (RS). The obtained results indicated that the synthesized mixture consisted of nanoscale HA and $CaCO_3$ with uniform distribution throughout the composite. TTCP was observed in the air quenching samples when the calcination temperature was above 1185°C. With the increase of the calcination temperature, the amount of the intermediate products in the air quenching samples decreased and cannot be detected when calcination temperature reached 1450°C. Unexpectedly, the mixture of HA and calcium oxide was observed in the furnace cooling samples. Clearly, the calcination temperature and cooling methods are critical for the synthesis of high-purity TTCP. The results indicate that the nanosize of precursors can decrease the calcination temperature, and TTCP can be calcinated by low temperature.

1. Introduction

Monoclinic tetracalcium phosphate ($CaO(PO_4)_2$, TTCP), a kind of calcium phosphates which can be formed in the (CaO–P_2O_5) system at high temperature (>1300°C), is the only calcium phosphate phase with a Ca/P ratio greater than stoichiometric hydroxyapatite ($Ca_{10}(PO_4)_6(OH)_2$, HA). It shows moderate reactivity and solubility when combined with acidic calcium phosphates such as dicalcium phosphate anhydrous ($CaHPO_4$, DCPA, monetite) or dicalcium phosphate dihydrate ($CaHPO_4{\cdot}2H_2O$, DCPD, brushite). Therefore, TTCP has been widely used in self-setting calcium phosphate cements for bone regeneration, which consequently leads to the formation of HA in physiologic conditions [1–4].

The preparation of high-purity TTCP powders, an important raw material in the field of calcium phosphate bone cements, is the key to fabricate calcium phosphate bone cements (CPC) with desirable performance in vivo. Regarding the synthesis of TTCP, there are mainly two approaches. One is direct solid-state reaction and the other is wet process reaction. The solid-state reaction at high temperature has been widely used in the synthesis of TTCP [5–7]. This technique is usually based on the use of mixtures of calcium carbonate ($CaCO_3$) and dicalcium phosphate anhydrate ($CaHPO_4$) (Ca/P ratio of 2), followed by heating at 1450–1500°C for 6–12 h. However, the treatment time of this method is long and the obtained products are generally not pure, including other phases such as calcium phosphates and even calcium oxide [8–11]. Dai et al. [12] have prepared the HA and CaO doped TTCP by this method. On the other hand, wet process reaction mainly refers to coprecipitation-solid state reaction. The nanoscale hydroxyapatite-calcium carbonate powder mixture was firstly prepared by the coprecipitation, followed by calcination at 1500°C to obtain TTCP. In this way, high purity TTCP can be obtained at low

temperature by this time-saving and facile method which most likely resulted from the small dimension effect and surface effect of precipitated nanoparticles. In this study, we present a modified method for the preparation of pure TTCP based on nanosized powder mixtures of the calcium carbonate and hydroxyapatite by wet process reaction and then calcinated at different temperature. The phase transition resulting from the synthesizing process of TTCP was investigated by TEM, DTA-TG, XRD, FT-IR, and RS. The reaction mechanism was explored, and the optimal temperature for synthesis of TTCP ceramics with high purity was obtained.

2. Materials and Methods

2.1. Preparation of Sample. Calcium nitrate ($Ca(NO_3)_2{\cdot}4H_2O$) (Shanghai ShanPu Chemical Reagent Co., Ltd., China), diammonium hydrogen phosphate ($(NH_4)_2HPO_4$) (Tianjin Dengke Chemical Reagent Co. Ltd., China), ammonium carbonate ($(NH_4)_2CO_3$) (Tianjin Kermel Chemical Reagent Co., Ltd., China), and all other reagents used in the present study were of analytical grade.

The $(NH_4)_2HPO_4$ aqueous solution was slowly dropped into the stirred $Ca(NO_3)_2$ aqueous solution at water bath with the temperature of 60°C with a Ca/P molar ratio 2, and the pH for mature solution was adjusted to 11-12 by ammonium solution (26–28 vol%). After stirring for 2 h and precipitating for 24 h, pump filter was followed by washing 3 times with alcohol and drying in vacuum drier at 90°C for 24 h. After that the mixtures of nano-hydroxyapatite (n-HA) and nano-calcium carbonate (nano-$CaCO_3$) were acquired. The dried mixture was calcinated at 850°C, 1150°C, 1200°C, 1250°C, 1300°C, 1350°C, 1400°C, 1450°C, and 1500°C in an alumina crucible with a heating rate of 10°C/min and kept for 8 h. The product was rapidly cooled to room temperature by means of a lifting device in the air (about cooling rate 150°C/min).

In addition, some mixing powder calcinated at 1400°C, 1450°C, and 1500°C was cooled to room temperature in the furnace (about cooling rate 1°C/min).

2.2. Characterization of Sample. The morphology and microstructure of the precipitate mixtures were examined by transmission electron microscopy (TEM, JEM-2100 (URP), Jeol, Japan).

Powder XRD was used for phase analysis of the samples. The analysis was carried out on an X-ray diffractometer (XRD, D8ADVANCE, Bruker, Germany) equipped with a monochromator in the diffracted beam. The diffraction spectra were recorded from 15° to 60° using CuKa (wavelength = 0.154056 nm, 40 mA, 40 kV) radiation with step size 0.05° and step duration 1 s.

DTA-TG was conducted on the as-prepared powders (10 mg) to ascertain the thermal stability and decomposition temperature. DTA-TG was performed using thermal analysis-thermogravimetry (DTA-TG, STA409PC/4/H, NETZSCH, Germany) at a heating rate of 10°C min^{-1} from 50 to 1500°C in a static air atmosphere.

For excitation of Raman spectra the 514.5 nm line (20 mW) of an Ar^+-ion laser (inVia-Laser microscopic confocal Raman spectroscopy, Renishaw, UK) was used with resolution of 1 cm^{-1}.

Fourier transformed infrared (FTIR) spectra were recorded from KBr pellets by means of a Shimadzu-2000 FT-IR spectrometer (FT-IR, Shimadzu 2000, Shimadzu, Japan) with a spectral resolution of 2 cm^{-1}.

3. Results and Discussion

3.1. TEM Analysis. Figure 1(a) is the TEM images of synthesized nanocrystals and Figures 1(b) and 1(c) are the corresponding selected area electron diffraction analysis. It can be seen that the synthesized mixtures were nanosized rod-like crystals of calcium carbonate with size of 2–4 nm in diameter and 30–40 nm in length with an aspect ratio of ~12. Needle-like crystals of poorly crystallized hydroxyapatite were also observed with crystal size of 10–20 nm in diameter by 40–60 nm in length with an aspect ratio of ~3. n-HA and nano-$CaCO_3$ diffraction patterns were tested by selected area electron diffraction (SAED) as shown in Figures 1(b) and 1(c). Electron diffraction patterns were made of different radius of concentric circles, which clearly indicated that the substance was slightly crystallized crystal. The electron diffraction pattern composition was further determined by calculation of interplanar spacing based on

$$d = \frac{K}{R}, \tag{1}$$

where d is the crystal interplanar distance, K is the camera constant, and R is radius of diffractions rings. By comparing the calculated interplanar distance with standard PDF CARDS, it was confirmed that the synthetic crystals were composed of n-HA and n-CC. The corresponding (HKL) value of diffraction rings has been marked in Figures 1(b) and 1(c).

3.2. Thermal Analysis. Figure 2 shows the TG-DTA diagram of synthesized samples. It was observed that the weight loss was about 5.5% when the temperature changed from room temperature to 230°C, mainly caused by the loss of adsorbed water in the sample. Lattice water of the samples was removed in the temperature range of 230–570°C and the weight loss was shown to be about 2.5%. $CaCO_3$ was decomposed (equation (2)) in the temperature range of 570–850°C and weight loss was about 4.59%. In the range of 850–1185°C, the nonstoichiometric HA was decomposed into β-tricalcium phosphate (β-$Ca_3(PO_4)_2$, β-TCP) and HA (equation (3)) [13]. While the temperature exceeded 850°C, HA could react to form oxygen apatite ($Ca_{10}(PO_4)_6(OH)_{2-2x}O_x\square_x$, OHA) (equation (4)) [13, 14]. When reaction temperature was above 1050°C, $Ca_{10}(PO_4)_6(OH)_2$ could react to form β-TCP and TTCP (equation (5)) [13]; while the temperature exceeded 1350°C, β-TCP could transform into α-tricalcium phosphate (α-$Ca_3(PO_4)_2$, α-TCP) (equation (6)) [13]; meanwhile, the β-TCP and HA were formed by the reaction as shown in (3), which could also react to form α-TCP and TTCP in the temperature range of 1185–1255°C (equation (7)) [13]. Moreover, when the enough CaO existed in the calcination

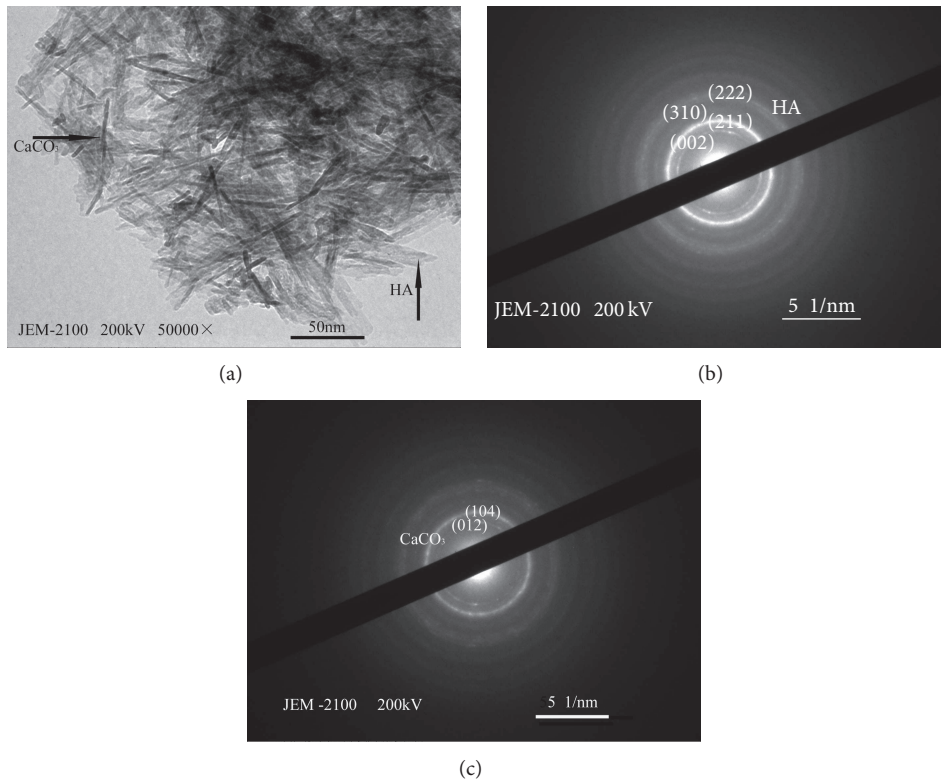

(a) (b) (c)

Figure 1: TEM images of the precipitates (a) and the selected area electron diffraction analysis (b, c).

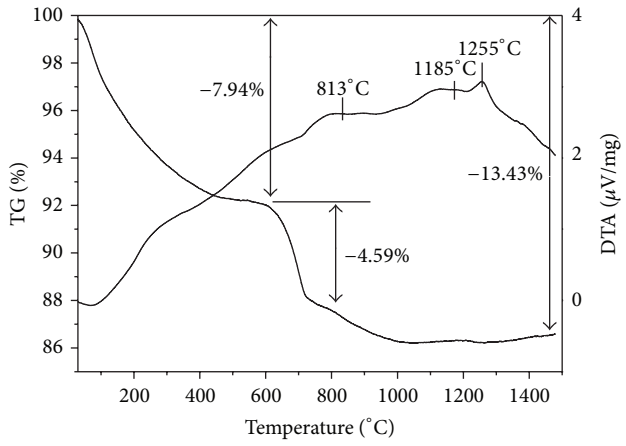

Figure 2: TG and DTA curves of synthetic sample.

samples, the final products TTCP could be formed by reaction shown in (8) and (9) [11, 13]. Consider the following:

$$\mathrm{CaCO_3} \longrightarrow \mathrm{CaO} + \mathrm{CO_2} \tag{2}$$

nonstoichiometric HA

$$\mathrm{Ca_{10-x}H_{2x}(PO_4)_6(OH)_2} \xrightarrow{>800^\circ\mathrm{C}} \beta\text{-}\mathrm{Ca_3(PO_4)_2} + \mathrm{Ca_{10}(PO_4)_6(OH)_2} \tag{3}$$

and stoichiometric HA

$$\mathrm{Ca_{10}(PO_4)_6(OH)_2} \xrightarrow{>850^\circ\mathrm{C}} \mathrm{Ca_{10}(PO_4)_6(OH)_{2-2x}O_x\square_x} \tag{4}$$

$$\mathrm{Ca_{10}(PO_4)_6(OH)_{2-2x}O_x\square_x} \xrightarrow{>1050^\circ\mathrm{C}} 2\beta\text{-}\mathrm{Ca_3(PO_4)_2} + \mathrm{Ca_4O(PO_4)_2} \tag{5}$$

$$\beta\text{-}\mathrm{Ca_3(PO_4)_2} + \mathrm{Ca_4O(PO_4)_2} \xrightarrow{>1350^\circ\mathrm{C}} 2\alpha\text{-}\mathrm{Ca_3(PO_4)_2} + \mathrm{Ca_4O(PO_4)_2} \tag{6}$$

$$\beta\text{-}\mathrm{Ca_3(PO_4)_2} + \mathrm{Ca_{10}(PO_4)_6(OH)_2} \xrightarrow{>1200^\circ\mathrm{C}} 2\alpha\text{-}\mathrm{Ca_3(PO_4)_2} + \mathrm{Ca_4O(PO_4)_2} \tag{7}$$

$$\alpha\text{-}\mathrm{Ca_3(PO_4)_2} + \mathrm{CaO} \longrightarrow \mathrm{Ca_4O(PO_4)_2} \tag{8}$$

$$\beta\text{-}\mathrm{Ca_3(PO_4)_2} + \mathrm{CaO} \longrightarrow \mathrm{Ca_4O(PO_4)_2} \tag{9}$$

3.3. XRD Analysis. Figure 3 shows the XRD patterns of the air-cooled quenching products sintered at different temperatures. It can be seen from Figures 3(a) and 3(b) that coprecipitation products were mainly composed of HA and calcium carbonate ($CaCO_3$), as evidenced by the characteristic peaks of HA (JCPDS-09-0432) at 2θ = 25.9°(002), 31.9°(211), 32.3°(112), 32.9°(300), 39.9°(310) and the characteristic peak

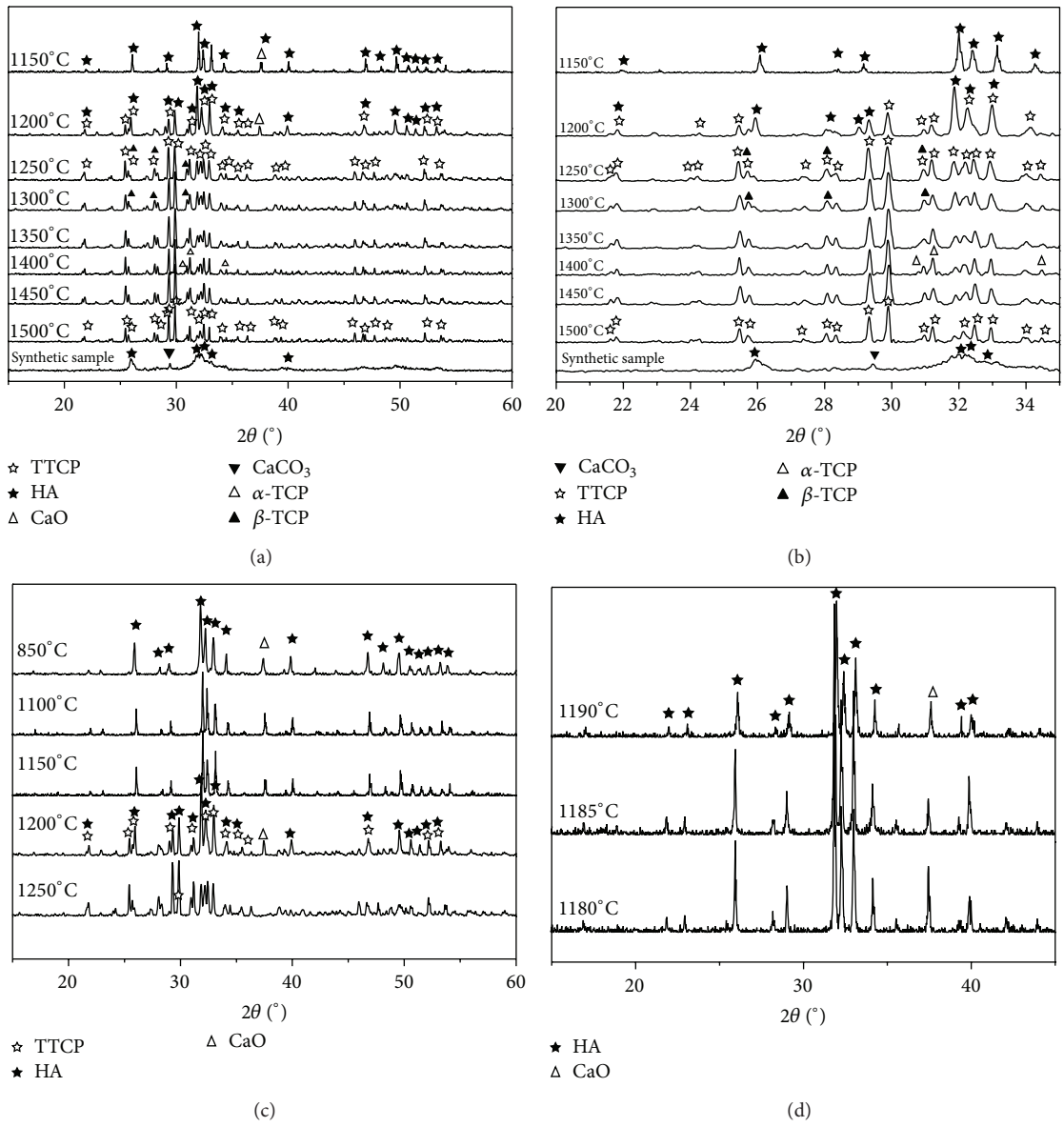

Figure 3: XRD patterns of synthetic samples after air-cooled quenching at various temperatures: full patterns (a, c $2\theta = 15–60^{\circ}$) and partial patterns (b $2\theta = 20–35^{\circ}$, d $2\theta = 15–45^{\circ}$), (a) synthetic sample, after air-cooled quenching at 1150–1500°C for 8 h, (b) partial patterns of (a), (c) after air-cooled quenching at 850°C, 1100°C, 1150°C, 1200°C, and 1250°C for 8 h, (d) after air-cooled quenching at 1180°C, 1185°C, and 1190°C for 8 h.

of $CaCO_3$ (JCPDS-29-0305) ($2\theta = 29.4^{\circ}(104)$) appearing in the XRD pattern of the samples. Moreover, the broad diffraction peaks revealed that both HA and $CaCO_3$ were poorly crystallized. After the calcination of coprecipitation products at 850°C, 1100°C, and 1150°C for 8 h (Figure 3(c)), respectively, mainly HA and calcium oxide (CaO, JCPDS-37-1497) remained. The absence of TTCP characteristic peaks indicated that the synthesis reaction of TTCP does not happen in this temperature range. The presence of characteristic peaks of the HA, TTCP, and CaO after calcination at 1200°C for 8 h showed that the calcination temperature between 1150°C and 1200°C resulted into the formation of TTCP phase, which corresponded to the results of DTA analysis, namely, crystal transition of TTCP about 1185°C. Figure 3(d) shows the XRD patterns of the products calcinated at 1180°C, 1185°C, and 1190°C for 8 h. When the temperature was varied from 1180 to 1185°C, the peak intensity of CaO at $2\theta = 37.4^{\circ}(200)$ and HA at $2\theta = 25.4^{\circ}$ decreased. Such phenomena may be due to the formation of a little amount of TTCP, causing an absence of characteristic peak of TTCP.

If the coprecipitation mixture was calcinated at 1250°C to 1500°C for 8 h followed by air-cooling, the characteristic peaks of the resultant products were at $21.8^{\circ}(121)$, $25.4^{\circ}(200)$, $25.7^{\circ}(130)$, $28.0^{\circ}(211)$, $28.3^{\circ}(211)$, $29.3^{\circ}(032)$, $29.8^{\circ}(040)$, 30.9° (-103), $31.2^{\circ}(221)$, 31.9° (-132), $32.1^{\circ}(113)$, 32.4° (-212), and $32.9^{\circ}(212)$, which agreed with the JCPDS pattern number

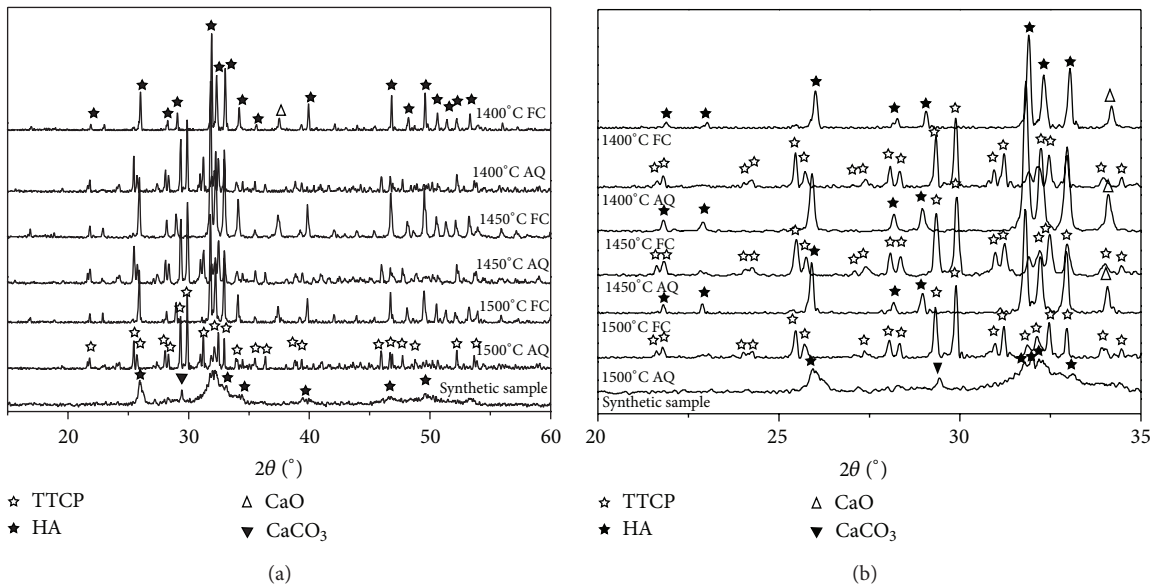

Figure 4: XRD patterns of the calcinations samples by different cooling methods: full patterns (a) and partial patterns (b). AQ indicates air quenching and FC indicates furnace cooling.

25-1137 of TTCP. Meanwhile, the disappearance of CaO characteristic peaks showed that the high-purity TTCP can be prepared with the temperature rising to more than 1250°C.

Figure 4 displays XRD patterns of samples by different cooling methods after the high temperature calcination. It was obvious that the furnace-cooled samples exhibited characteristic peak of calcium oxide at ca. 37.5° [14]; the other characteristic peaks at 25.9°, 31.8°, 32.2°, 32.9°, 34.1°, 39.8°, 46.7°, 48.1°, 49.2°, and 49.5° can be related to the peaks of HA phase. However, the characteristic peaks of TTCP and HA at 2θ = 31.8°, 32.2°, 32.9°, 32.2°, 46.7°, and 48.1° are relatively similar, which makes it quite difficult to identify the phase composition of this mixture, thereby confirming the previous conclusion that with the furnace cooling method pure TTCP cannot be obtained [15].

3.4. FT-IR Analysis. The fundamental vibration modes for the isolated PO_4^{3-} ion are designated as ν_1, ν_2, ν_3, and ν_4. Vibrations from the symmetric stretching motion of the P–O bonds corresponded to ν_1, while the bending vibrations corresponded to ν_2. The wavenumber of asymmetric stretching vibrations was represented as ν_3 and the wavenumber of O–P–O asymmetric bending vibrations was represented as ν_4 [16, 17].

Figure 5 shows the FT-IR spectra of the calcinated and air-cooled products. The peaks at 603 cm^{-1} and 567 cm^{-1} (ν_4) were assigned to the asymmetric bending vibration of PO_4^{3-} group in HA, the peaks at 1037 cm^{-1} and 1092 cm^{-1} (ν_3) was related to the antisymmetry stretching vibration of PO_4^{3-} group, and and the peak at 962 cm^{-1} (ν_1) represented the symmetry stretching vibration of PO_4^{3-} group. The stretching and bending vibrations of OH^- groups in HA appeared at about 3572 cm^{-1} and 635 cm^{-1}. Thus, the characteristics vibrations of PO_4^{3-} and OH^- indicated that HA existed in the synthetic sample. Peaks at 1637 cm^{-1} and 3431 cm^{-1} belonged to bending vibration and stretching vibration of surface adsorbed water in the synthetic sample, respectively. Peaks at 1386 cm^{-1} belonged to antisymmetric stretching vibration of NO_3^- in the residual samples. The antisymmetric stretching vibration and out-of-plane bending vibration of CO_3^{2-} group in $CaCO_3$ were at 857 cm^{-1} and 1481 cm^{-1}. The peak at 3644 cm^{-1} was related to stretching vibration of OH^- group in calcium hydroxide [15], which existed in the samples calcinated from temperature between 850°C and 1200°C for 8 h. This fact was evidenced by the OH band (at 3644 cm^{-1}), which was derived from $Ca(OH)_2$ formed through absorption of water by CaO [18]. The disappearance of peak at 3644 cm^{-1} and bending vibration of OH^- in HA at 635 cm^{-1} at the temperature above 1200°C indicated that calcium oxide and HA were obtained; thus they were consumed during reaction, which was too little to be detected. This phenomenon was consistent with characteristic diffraction peaks of calcium oxide in Figure 3, in which samples were calcinated from 850°C to 1200°C, respectively.

The peak at 3672 cm^{-1} was derived from the stretching vibration of OH^- group in HA. This peak existed in these samples calcinated from 850°C to 1400°C for 8 h. However, the peak intensity was gradually weakened and disappeared when the calcination temperature went up to 1450°C. This indicated that the calcinated samples contained a some of HA under 1450°C, which could be decomposed when calcination temperature was above 1450°C. When calcination temperature went up to 1450°C and 1500°C, the characteristic peaks of the TTCP at 454 cm^{-1}, 470 cm^{-1}, 501 cm^{-1}, 570 cm^{-1}, 593 cm^{-1}, 601 cm^{-1}, 621 cm^{-1}, and 930–1100 cm^{-1} appeared, corresponding to the vibration mode showed in Table 1.

Figure 6 displays FT-IR spectra of the calcination sample by different cooling methods. The three quenched samples

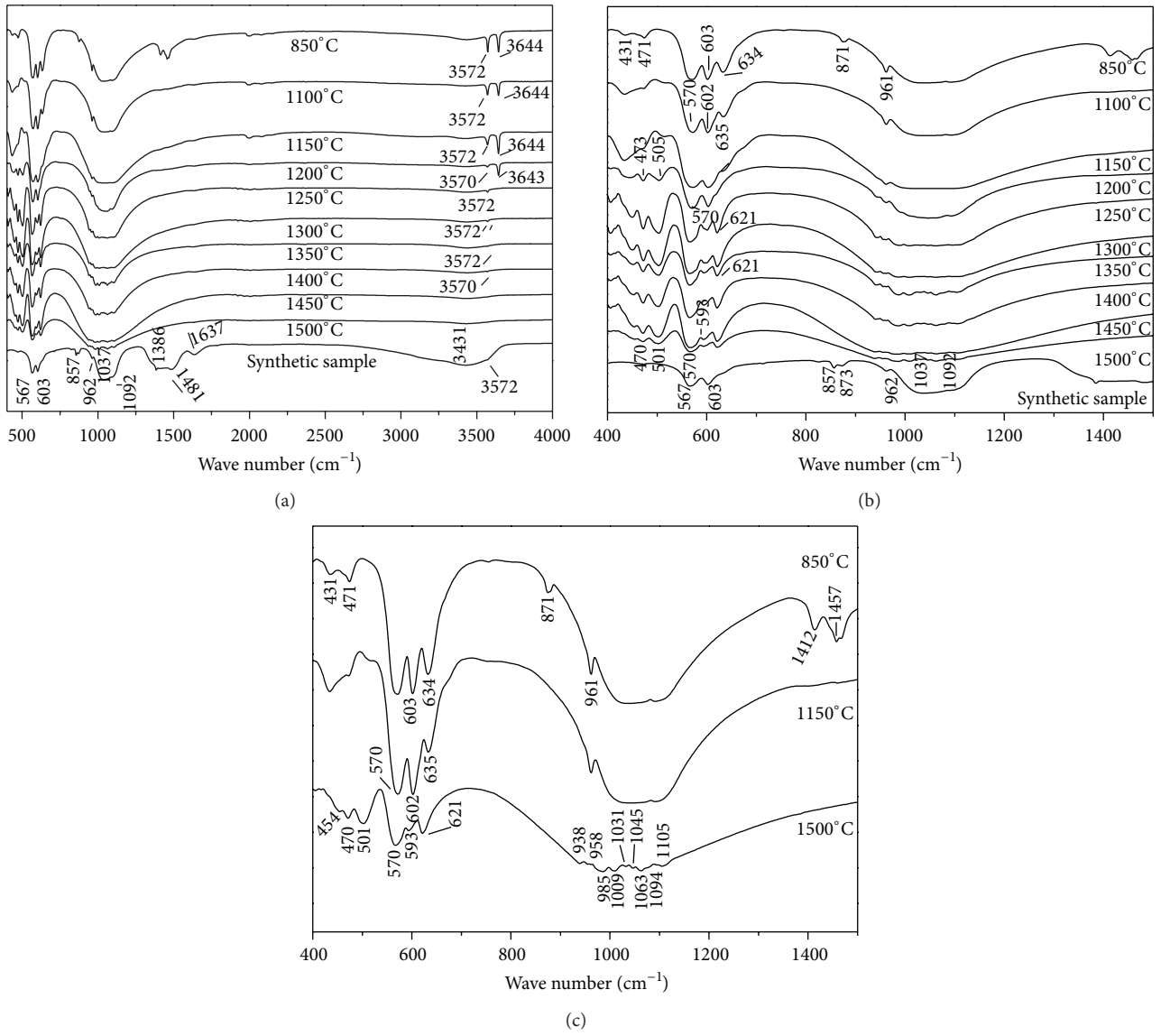

Figure 5: FT-IR spectra of synthetic samples in air-cooled quenching at various temperatures: full spectrum (a) and partial spectrum (b, c).

scarcely contained OH^- stretching vibration, and only the quenched samples calcinated at 1400°C exhibited very weak OH^- stretching vibration at ca. 3572 cm^{-1}; these furnace cooling samples exhibited sharp peaks of OH^- stretching vibration in $Ca(OH)_2$ at 3643 cm^{-1}; sharp peaks of OH^- stretching vibration in HA at 3572 cm^{-1} and 635 cm^{-1}, and asymmetric stretching vibration of CO_3^{2-} in CaO, the calcium carbonate was derived from reaction of $Ca(OH)_2$ and CO_2 in the air. This result revealed that TTCP was decomposed into HA and CaO during the furnace cooling.

3.5. RS Analysis. Figure 7 shows the Raman spectra of synthetic samples by air-cooled quenching at various temperatures. As can be seen from Figures 7(b) and 7(g), the samples have the symmetric bending vibrations ν_2 of PO_4^{3-} at 429 cm^{-1}, the asymmetric bending vibrations ν_4 of PO_4^{3-} at 586 cm^{-1}, the symmetric stretching vibrations ν_1 of PO_4^{3-} about at 960 cm^{-1}, and the symmetric stretching vibrations of CO_3^{2-} at 1084 cm^{-1}. Obviously, with calcination temperatures increasing from 1200°C to 1500°C, the characteristic peaks of PO_4^{3-} at 407 cm^{-1}, 448 cm^{-1}, 480 cm^{-1}, 586 cm^{-1}, 958 cm^{-1}, 1042 cm^{-1}, 1075 cm^{-1}, and 1095 cm^{-1} of PO_4^{3-} were observed in the spectra of the calcinations samples. The OH^- stretching vibration at about 3570 cm^{-1} disappeared gradually, and the HA in the samples completely transformed into TTCP with the increase of calcination temperatures.

Figure 7(g) shows the Raman spectra of the samples calcinated from 850°C to 1200°C. The OH^- Raman peaks from HA and $Ca(OH)_2$ were clearly observed at 3571 cm^{-1} and 3619 cm^{-1}, respectively. However, the two Raman peaks

Table 1: Vibrational wave numbers [cm^{-1}] of samples.

	Raman λ_0 = 514.5 nm	FT-IR KBr	Assignments
1400~1500°C ×8 h	327		Lattice modes
	390, 408, 448, 481	454, 470, 501	ν_2, PO_4^{3-} bands in TTCP, symmetric bending vibrations mode
	555, 565, 577, 598, 608, 616	570, 593, 621	ν_4, PO_4^{3-} bands in TTCP, asymmetric bending vibrations mode
	941, 948, 957, 963	938, 958	ν_1, PO_4^{3-} bands in TTCP, symmetric stretching mode
	992, 1010, 1027, 1046, 1075, 1095, 1122, 1135	985, 1009, 1031, 1045, 1063, 1074, 1094, 1105	ν_3, PO_4^{3-} bands in TTCP, asymmetric stretching mode
850–1150°C ×8 h	430, 445	431, 471	ν_2, PO_4^{3-} bands in HA
	579, 590, 607	604	ν_4, PO_4^{3-} bands in HA
		634	Vibrational mode of OH^-
		871	Out-of-plane bending vibrations of CO_3^{2-}
	961	961	ν_1, PO_4^{3-} bands in HA
	1028, 1046, 1075, 1123	1025, 1091	ν_3, PO_4^{3-} bands in HA
	1085		Symmetric stretching of CO_3^{2-}
		1412, 1452, 1467	Asymmetric stretching of CO_3^{2-}
	3572	3572	OH^- stretching vibration (in HA)
	3619	3643	OH^- stretching vibration (in $Ca(OH)_2$)

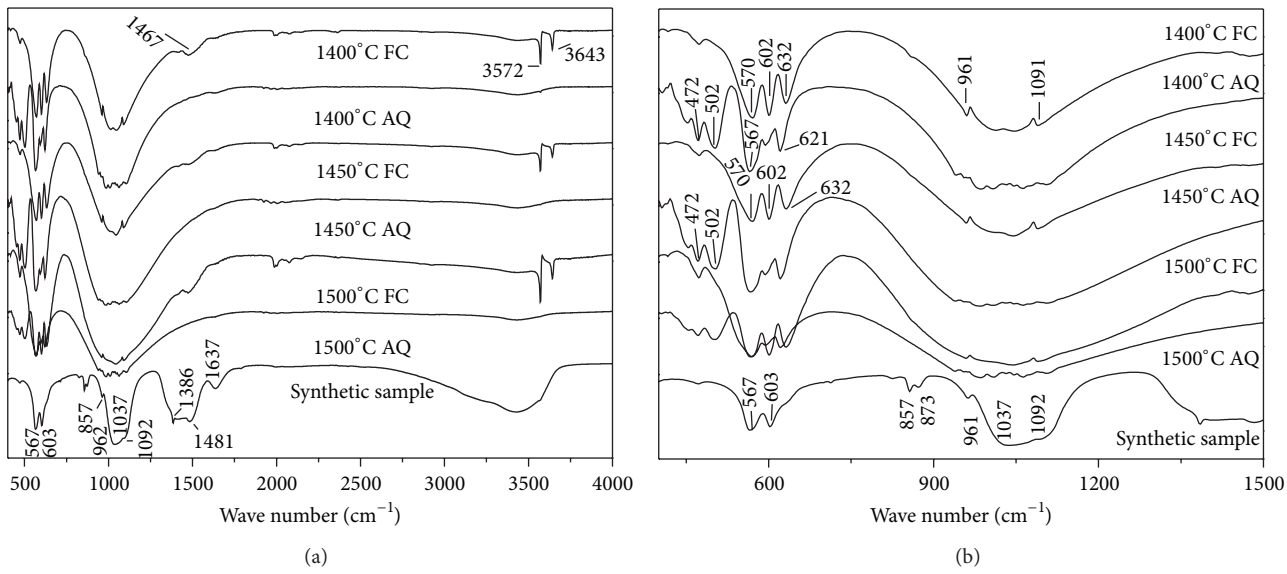

Figure 6: FT-IR spectra of the samples calcinated by different cooling methods: full spectrum (a) and partial spectrum (b). AQ indicates air quenching and FC indicates furnace cooling.

were gradually weakened with the temperature increasing from 850°C to 1200°C; finally the Raman peak at 3619 cm^{-1} disappeared and only a strong OH^- Raman peak of HA at 3571 cm^{-1} was retained when calcinated at 1250°C. The peak at 3571 cm^{-1} also gradually decreased with the increasing temperature, which was almost invisible at 1400°C, and completely disappeared when the temperature reached 1450°C. The results suggested the formation of TTCP resulting from the reaction between CaO and HA with the calcination temperature increased, as given by the following equations:

$$2CaO + Ca_{10}(PO_4)_6(OH)_2 \longrightarrow 3Ca_4O(PO_4)_2 + H_2O \quad (10)$$

Equation (2) represented the existing reaction at 850°C, in which the appearance of the OH^- Raman peak in $Ca(OH)_2$ was observed, which resulted from the reaction of calcium

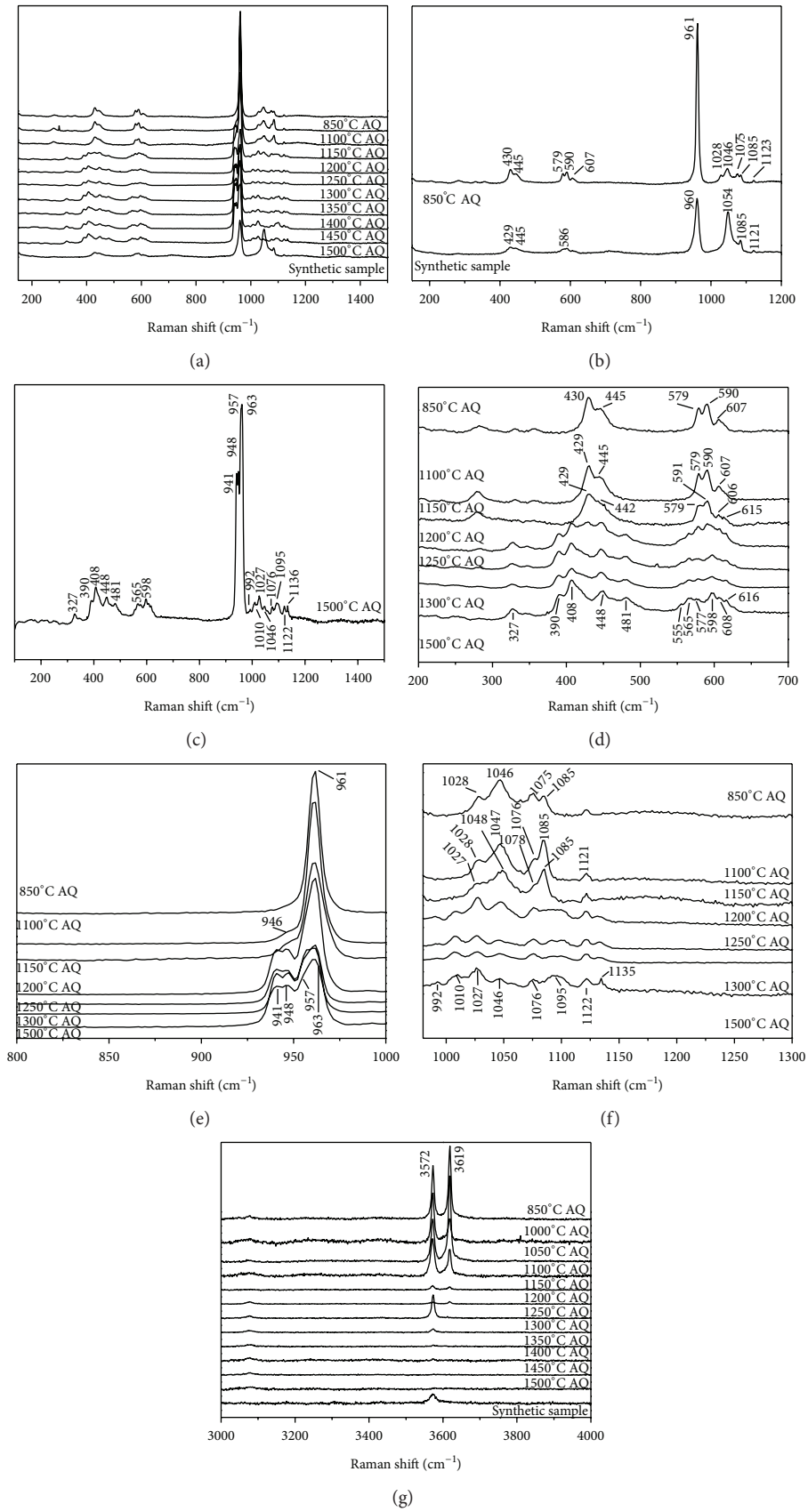

Figure 7: Raman spectra of synthetic samples by air-cooled quenching at various temperatures.

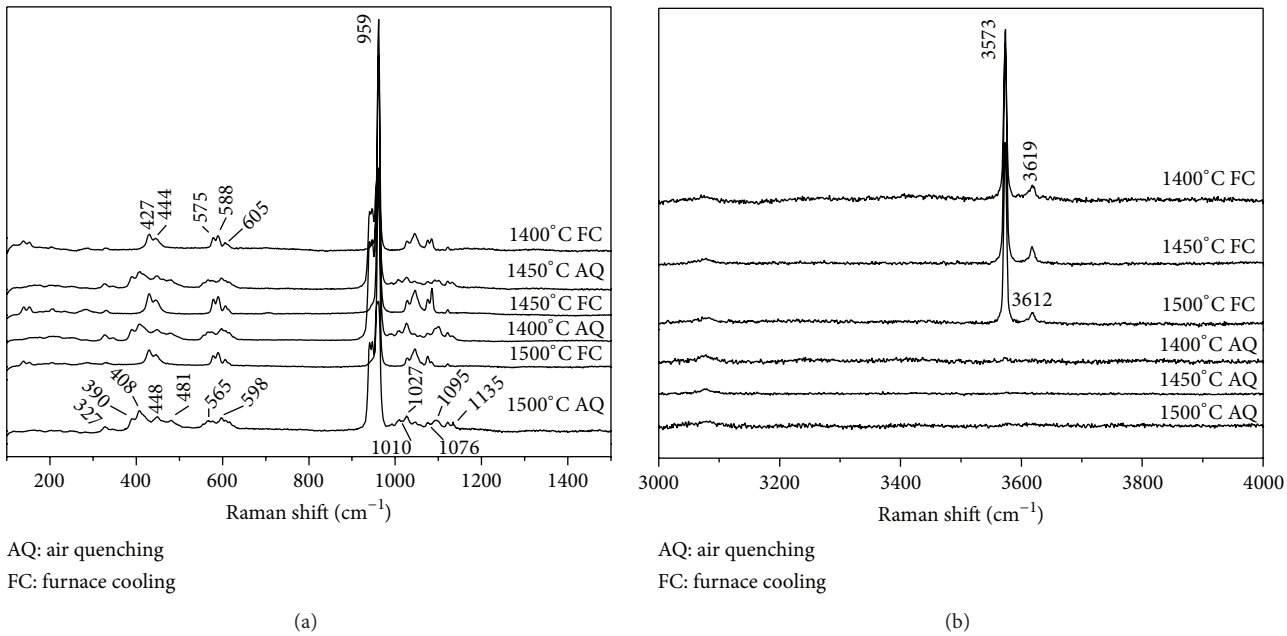

Figure 8: Raman spectra of the samples calcinated by different cooling methods: Raman shift 100–1500 cm^{-1} (a) and Raman shift 3000–4000 cm^{-1} (b).

oxide and the water in the air. Equation (10) represented the reaction occurring when calcination temperature was up to 1150°C and above 1150°C, which was evidenced by the change of Raman peak of the sample. As can be seen from Figure 7(d), the symmetric bending vibration peaks ν_2 of PO_4^{3-} appeared at 389 cm^{-1} and 407 cm^{-1}, and the original characteristic peak at 429 cm^{-1} was weakened at 1200°C. The Raman peak at 429 cm^{-1} disappeared with the increase of temperature. Meanwhile, the Raman spectrum showed that the asymmetric bending vibrations peaks ν_4 of PO_4^{3-} at 578 cm^{-1}, 589 cm^{-1}, and 606 cm^{-1} were splitted into six peaks at 555 cm^{-1}, 565 cm^{-1}, 576 cm^{-1}, 597 cm^{-1}, 608 cm^{-1}, and 616 cm^{-1}. As can be seen from Figure 7(e), the symmetric stretching vibration of PO_4^{3-} (ν_1) appeared at 946 cm^{-1} when it is at 1150°C, then was splitted into four intense distinct peaks at 941 cm^{-1}, 948 cm^{-1}, 957 cm^{-1} and 963 cm^{-1} when it was increased to 1200°C. Meanwhile, the appearance of lattice vibration Raman peak of TTCP at about 326 cm^{-1} in the calcination samples was confirmed. The reaction showed as (10) did not cease until it was up to 1450°C, which can be demonstrated from the disappearance of OH^- characteristic Raman peak at 1450°C. In addition, the DTA curve in Figure 2 showed that the endothermic peaks of crystal structure transition began to occur at 1185°C in the sample, and it can be confirmed that the initial reaction temperature of (2) was between 1150 and 1200°C.

Figure 8 is the Raman spectra patterns of synthetic samples calcinated at 1500°C, 1450°C, and 1400°C and then cooled by two different methods, and the changes of Raman peaks are listed in Table 2. The Raman test showed that the furnace cooling samples led to the presence of the characteristic peak of OH^- in HA at about 3573 cm^{-1} and characteristic peak of OH^- in $Ca(OH)_2$ at about 3619 cm^{-1}. This result revealed that the sample was a mixture of HA and CaO. Posset et al. [17] presented that the Raman peaks of PO_4^{3-} symmetric stretching vibration ν_1 were its characteristic peak. This peak, splitting or not, gave a major evidence for the difference between TTCP and HA. Only an intense distinct Raman peak in the range between 960 and 940 cm^{-1} and the spliting peak in the samples by furnace cooling could not be observed, indicating that TTCP can't be obtained by this cooling method. While the air-quenching samples exhibited four intense distinct peaks at this range, which demonstrated that TTCP was only product by air quenching.

3.6. Discussion. At present, common methods for the synthesis of TTCP are limited to solid-state reactions at high temperatures, based on powder mixtures of $CaCO_3$ and dicalcium phosphate anhydrate ($CaHPO_4$) [19], in which the particle size of powder is in the micron level, with calcination temperature higher than 1450°C. Though the reaction time was long enough for 6–12 h, even up to 15–24 h [9, 12, 20], the products may still contain HA or OHA. Sargin et al. [15] reported several attempts to lower the required processing temperature for the TTCP synthesis using different combinations of various starting products. By varying the process temperatures, they showed that HA or TCP appeared as intermediate products at lower temperatures in all reactions. Although this reaction enabled the formation of TTCP even at 1200°C, which was much lower than previous report, the purity was lower than that in the product obtained at 1350°C. Jalota et al. [6] investigated $NH_4H_2PO_4$ and $Ca(CH_3COO)_2{\cdot}H_2O$ powders to further reduce the temperature required for the preparation of phase-pure TTCP.

Table 2: Raman shift [cm^{-1}] of the calcinations samples by different cooling methods.

	1400~1500°C ×8 h, air quenching	1400~1500°C ×8 h, furnace cooling	Assignments
Raman $\lambda_0 = 514.5$ nm	327		Lattice modes (TTCP)
	390, 408, 448, 481	427, 444	ν_2, PO_4^{3-} bands, symmetric bending vibrations mode
	555, 565, 577, 598, 608, 616	575, 588, 605	ν_4, PO_4^{3-} bands, asymmetric bending vibrations mode
	941, 948, 957, 963	959	ν_1, PO_4^{3-} bands, symmetric stretching mode
	992, 1010, 1027, 1046, 1075, 1095, 1122, 1135	1026, 1040, 1072, 1121	ν_3, PO_4^{3-} bands, asymmetric stretching mode
		3573	OH^- stretching vibration (in HA)
		3619	OH^- stretching vibration (in $Ca(OH)_2$)

However, the method was suitable only for the synthesis of HA-seeded TTCP powders, which were very sensitive and easily transformed into HA by mechanochemical activation [21]. Romeo and Fanovich [7] studied a solid-state reaction of $CaCO_3$ and $(NH_4)_2HPO_4$ powders mixed with a Ca/P ratio of 2 and ball-milled prior to thermal treatment. The smaller crystallite size of the milled powders increased the reactivity and significantly improved the purity of the final product.

It is well known that the driving force of calcination process comes from the decrease of systematic free energy, including increase in particles bonding areas and the total specific surface area, decrease in surface free energy, void volume and area reduction, the lattice distortion's elimination, and so forth. Due to the surface and interface effect, small size effect of nanoparticles, the driving force of grain growth is very big, decades or even one hundred times that of ordinary powder calcination process. So, this research shows that it is easy to obtain pure TTCP by using the wet method for synthesizing the mixture of nanoscale HA and calcium carbonate, followed by high temperature treatment.

According to [20], when the temperature was increased, the dehydration or decomposition of the prior formed HA will occur to form weak crystal oxyapatite ($Ca_{10}(PO_4)_6(OH)_{2-2x}O_x\square_x$, OHA) (equations (4), (11)), $x = 0 - l$, and $\square$ is oxygen vacancy [22]. As the thermodynamic metastable equilibrium phase [14], $Ca_{l0}(PO_4)_6O$ ($x = l$, OA) was less stable, easy to decompose into tricalcium phosphate ($Ca_3(PO_4)_2$, TCP) and CaO (equation (12)). When CaO is relatively excessive in the reaction system, TCP reacted with CaO rapidly with the extension of heat preservation time and TTCP was obtained (equation (9)). In this study, the synthetic mixture of nanoscale HA and CC crystals were calcinated at different temperature. Only characteristic diffraction peaks of HA and CaO were obtained at temperature lower than 1150°C as shown in Figure 3, in which the characteristic peak of TTCP appeared at 1200°C. Meantime, the intensity of characteristic peaks from HA and CaO decreased; the characteristic peaks of CaO disappeared at 1250°C, which might not be detected in the XRD pattern due to the sensitivity limitations of the instruments. However, as seen in Figure 7(g), the strong Raman peaks of the OH^- in HA showed that it still contained HA at 1250°C. When the calcination temperature was higher than 1250°C, the Raman peak intensities of OH^- in HA gradually decreased, which however can be still distinguished at 1400°C. The Raman peak of OH^- disappeared at 1450°C and pure TTCP could be obtained in this case. The results showed that there was no α-TCP or β-TCP in this experimental process, except for the intermediate products of HA and CaO. When the temperature is higher than 1150°C, the reaction between HA and CaO occurred directly and TTCP was formed (equation (10)):

$$Ca_{10}(PO_4)_6(OH)_2 \longrightarrow Ca_{10}(PO_4)_6O + H_2O \quad (11)$$

$$Ca_{10}(PO_4)_6O \longrightarrow 3Ca_3(PO_4)_2 + CaO \quad (12)$$

In the preparation process of TTCP by high temperature solid-state reaction, cooling methods are of great importance. After heating, the samples must be rapidly quenched to room temperature in order to avoid the formation of undesired secondary phases such as HA, CaO, $CaCO_3$, and β-TCP. Bohner [23] pointed out that TTCP could be obtained by a solid-state reaction at high temperatures (typically 1400°C), usually between equimolar quantities of DCPD and $CaCO_3$. This reaction should be carried out in a dry atmosphere of vacuum, or with rapid cooling to prevent TTCP to uptake of water from the environment which might lead to the formation of HA. Guo et al. [11, 20] investigated the effect of cooling rate on the purity of TTCP prepared by high temperature solid-state reaction. The results indicated that the purity of TTCP depended decisively on the cooling rate after TTCP was sintered at 1500°C for 15 h. Quenching in air was propitious for the formation of pure TTCP, while cooling in furnace will cause the decomposition of TTCP and less TTCP obtained. It showed that cooling rate was a key to the synthesis of TTCP by solid-state reaction.

4. Conclusion

The high-purity TTCP was prepared via coprecipitation-solid state reaction and calcination of n-HA and nano-$CaCO_3$. In contrast, mixtures with good homogenization and weak crystallinity of nanocrystals were obtained using wet method reaction. In the latter preparation method, nano-$CaCO_3$ and n-HA with high activity can be prepared after coprecipitation. The enhanced reactivity of the mixtures was related to both the loss of crystallinity of the reactants and the generation of defects at the surface of nanocrystals. It was established that the mixture of TTCP, HA, and CaO can be obtained by 8 h of heat treatment at temperature above 1200°C, and the pure TTCP can be obtained if the temperature was above or equal to 1450°C.

Conflict of Interests

The authors declare that there is no conflict of interests regarding the publication of this paper.

Acknowledgments

This work was financially supported by the National Natural Science Foundation of China (no. U1304820), the Education Department of Henan Province Basic Research Program (no. 13A430331), and Doctoral Program of Henan Polytechnic University (B2009-36).

References

[1] S. Takagi and L. C. Chow, "Formation of macropores in calcium phosphate cement implants," *Journal of Materials Science: Materials in Medicine*, vol. 12, no. 2, pp. 135–139, 2001.

[2] Y. Ueyama, K. Ishikawa, T. Mano et al., "Initial tissue response to anti-washout apatite cement in the rat palatal region: comparison with conventional apatite cement," *Journal of Biomedical Materials Research*, vol. 55, no. 4, pp. 652–660, 2001.

[3] C. Liu, H. Shao, F. Chen, and H. Zheng, "Effects of the granularity of raw materials on the hydration and hardening process of calcium phosphate cement," *Biomaterials*, vol. 24, no. 23, pp. 4103–4113, 2003.

[4] L. Medvecky, M. Giretova, and T. Sopcak, "Preparation and properties of tetracalcium phosphate-monetite biocement," *Materials Letters*, vol. 100, pp. 137–140, 2013.

[5] Y. Matsuya, S. Matsuya, J. M. Antonucci, S. Takagi, L. C. Chow, and A. Akamine, "Effect of powder grinding on hydroxyapatite formation in a polymeric calcium phosphate cement prepared from tetracalcium phosphate and poly(methyl vinyl ether-maleic acid)," *Biomaterials*, vol. 20, no. 7, pp. 691–697, 1999.

[6] S. Jalota, A. C. Tas, and S. B. Bhaduri, "Synthesis of HA-seeded TTCP ($Ca_4(PO_4)_2O$) powders at 1230°C from $Ca(CH_3COO)_2{\cdot}H_2O$ and $NH_4H_2PO_4$," *Journal of the American Ceramic Society*, vol. 88, no. 12, pp. 3353–3360, 2005.

[7] H. E. Romeo and M. A. Fanovich, "Synthesis of tetracalcium phosphate from mechanochemically activated reactants and assessment as a component of bone cements," *Journal of Materials Science: Materials in Medicine*, vol. 19, no. 7, pp. 2751–2760, 2008.

[8] V. V. Samuskevich, N. K. Belous, and L. N. Samuskevich, "Sequence of solid-state transformations during heat treatment of $CaCO_3$ + $CaHPO_4$ mixtures," *Inorganic Materials*, vol. 39, no. 5, pp. 520–524, 2003.

[9] J. E. Barralet, L. Grover, T. Gaunt, A. J. Wright, and I. R. Gibson, "Preparation of macroporous calcium phosphate cement tissue engineering scaffold," *Biomaterials*, vol. 23, no. 15, pp. 3063–3072, 2002.

[10] A. Hoshikawa, N. Fukui, A. Fukuda et al., "Quantitative analysis of the resorption and osteoconduction process of a calcium phosphate cement and its mechanical effect for screw fixation," *Biomaterials*, vol. 24, no. 27, pp. 4967–4975, 2003.

[11] D. Guo, K. Xu, and Y. Han, "Influence of cooling modes on purity of solid-state synthesized tetracalcium phosphate," *Materials Science and Engineering B*, vol. 116, no. 2, pp. 175–181, 2005.

[12] H. Dai, Y. Yan, Y. Wang, S. Li, and X. Jiang, "Study on preparation of tetracalcium phosphate powder," *Bulletin of the Chinese Ceramic Society*, vol. 21, p. 56, 2002 (Chinese).

[13] H. Aoki, *Science and Medical Applications of Hydroxyapatite*, Takayama Press System Center, JAAS, Tokyo, Japan, 1991.

[14] F.-H. Lin, C.-J. Liao, K.-S. Chen, and J.-S. Sun, "Thermal reconstruction behavior of the quenched hydroxyapatite powder during reheating in air," *Materials Science and Engineering C*, vol. 13, no. 1-2, pp. 97–104, 2000.

[15] Y. Sargin, M. Kizilyalli, C. Telli, and H. Güler, "A new method for the solid-state synthesis of tetracalcium phosphate, a dental cement: x-ray powder diffraction and IR studies," *Journal of the European Ceramic Society*, vol. 17, no. 7, pp. 963–970, 1997.

[16] A. Jillavenkatesa and R. A. Condrate Sr., "The infrared and raman spectra of tetracalcium phosphate ($Ca_4P_2O_9$)," *Spectroscopy Letters*, vol. 30, no. 8, pp. 1561–1570, 1997.

[17] U. Posset, E. Löcklin, R. Thull, and W. Kiefer, "Vibrational spectroscopic study of tetracalcium phosphate in pure polycrystalline form and as a constituent of a self-setting bone cement," *Journal of Biomedical Materials Research*, vol. 40, no. 4, pp. 640–645, 1998.

[18] A. Ślósarczyk, C. Paluszkiewicz, M. Gawlicki, and Z. Paszkiewicz, "The FTIR spectroscopy and QXRD studies of calcium phosphate based materials produced from the powder precursors with different Ca/P ratios," *Ceramics International*, vol. 23, no. 4, pp. 297–304, 1997.

[19] C. Moseke and U. Gbureck, "Tetracalcium phosphate: synthesis, properties and biomedical applications," *Acta Biomaterialia*, vol. 6, no. 10, pp. 3815–3823, 2010.

[20] D. Guo, K. Xu, and Y. Han, "Phase transition of synthesizing tetra calcium phosphate in a solid-state reaction," *Journal of Inorganic Materials*, vol. 20, p. 317, 2005 (Chinese).

[21] U. Gbureck, J. E. Barralet, M. Hofmann, and R. Thull, "Mechanical activation of tetracalcium phosphate," *Journal of the American Ceramic Society*, vol. 87, no. 2, pp. 311–313, 2004.

[22] R. B. Heimann, H. V. Tran, and P. Hartmann, "Laser-Raman and Nuclear Magnetic Resonance (NMR) studies on plasma-sprayed hydroxyapatite coatings: influence of bioinert bond coats on phase composition and resorption kinetics in simulated body fluid," *Materialwissenschaft und Werkstofftechnik*, vol. 34, no. 12, pp. 1163–1169, 2003.

[23] M. Bohner, "Calcium orthophosphates in medicine: from ceramics to calcium phosphate cements," *Injury*, vol. 31, no. 4, pp. D37–D47, 2000.